Journal of Biomechanics 61 (2017) 250–257

Contents lists available at ScienceDirect

Journal of Biomechanics

journal homepage: www.elsevier.com/locate/jbiomech
www.JBiomech.com

Short communication

Incorporating the length-dependent passive-force generating muscle properties of the extrinsic finger muscles into a wrist and finger biomechanical musculoskeletal model

Benjamin I. Binder-Markey [a,b,c], Wendy M. Murray [a,b,c,d,e,*]

[a] Dept. of Biomedical Engineering, Northwestern University, Evanston, IL, USA
[b] Dept. of Physical Therapy and Human Movement Sciences, Northwestern University, Chicago, IL, USA
[c] Shirley Ryan AbilityLab (formerly Rehabilitation Institute of Chicago), Chicago, IL, USA
[d] Edward Hines Jr., VA Hospital, Hines, IL, USA
[e] Dept. of Physical Medicine & Rehabilitation, Northwestern University, Chicago, IL, USA

ARTICLE INFO

Article history:
Accepted 13 June 2017

Keywords:
Passive torque
Hand
Finger
Wrist
Extrinsic finger muscles
Musculoskeletal modeling

ABSTRACT

Dynamic movement trajectories of low mass systems have been shown to be predominantly influenced by passive viscoelastic joint forces and torques compared to momentum and inertia. The hand is comprised of 27 small mass segments. Because of the influence of the extrinsic finger muscles, the passive torques about each finger joint become a complex function dependent on the posture of multiple joints of the distal upper limb. However, biomechanical models implemented for the dynamic simulation of hand movements generally don't extend proximally to include the wrist and distal upper limb. Thus, they cannot accurately represent these complex passive torques. The purpose of this short communication is to both describe a method to incorporate the length-dependent passive properties of the extrinsic index finger muscles into a biomechanical model of the upper limb and to demonstrate their influence on combined movement of the wrist and fingers. Leveraging a unique set of experimental data, that describes the net passive torque contributed by the extrinsic finger muscles about the metacarpophalangeal joint of the index finger as a function of both metacarpophalangeal and wrist postures, we simulated the length-dependent passive properties of the extrinsic finger muscles. Dynamic forward simulations demonstrate that a model including these properties passively exhibits coordinated movement between the wrist and finger joints, mimicking tenodesis, a behavior that is absent when the length-dependent properties are removed. This work emphasizes the importance of incorporating the length-dependent properties of the extrinsic finger muscles into biomechanical models to study healthy and impaired hand movements.
Published by Elsevier Ltd.

1. Introduction

The forces produced by soft tissue structures that surround a joint (including passive muscles) play a crucial role in the control and stabilization of dynamic movements of low mass and inertia systems. Experimental work on biomechanical systems ranging from insect legs to human wrists (Charles and Hogan, 2012; Hooper et al., 2009; Souza et al., 2009; Wu et al., 2012) has demonstrated that passive viscoelastic forces, and the joint torques that result, influence dynamic movement trajectories of low mass systems more than the momentum and inertia of the segments.

Comprised of 27 bones with masses ranging between 0.002 and 0.04 kg (Le Minor and Rapp, 2001; McFadden and Bracht, 2003; Mirakhorlo et al., 2016; Saul et al., 2015), the hand is a small mass and inertia system. As a result, the inclusion of passive viscoelastic forces are critical for the simulation of controlled dynamic movements of the hand and fingers (Esteki and Mansour, 1997; Kamper et al., 2002). Passive viscoelastic forces in the hand are produced by soft tissue structures, either those that act within the hand (e.g., ligaments, joint capsules, skin, and intrinsic finger muscles) or the extrinsic finger muscles, which originate proximally, cross the wrist, and attach distally on the fingers (Knutson et al., 2000; Kuo and Deshpande, 2012). Because the force a muscle produces depends on length, it varies as a function of the posture of every joint the muscle crosses. Thus, forces produced by the passive extrinsic finger muscles are a complex, multi-dimensional function of joint postures of the distal upper limb (Bhardwaj

* Corresponding author at: Arms + Hands Lab (21st Floor), Shirley Ryan AbilityLab, 355 E. Erie St., Chicago, IL 60611, USA. Fax: +1 (312) 238 2208.
E-mail address: w-murray@northwestern.edu (W.M. Murray).

http://dx.doi.org/10.1016/j.jbiomech.2017.06.026
0021-9290/Published by Elsevier Ltd.

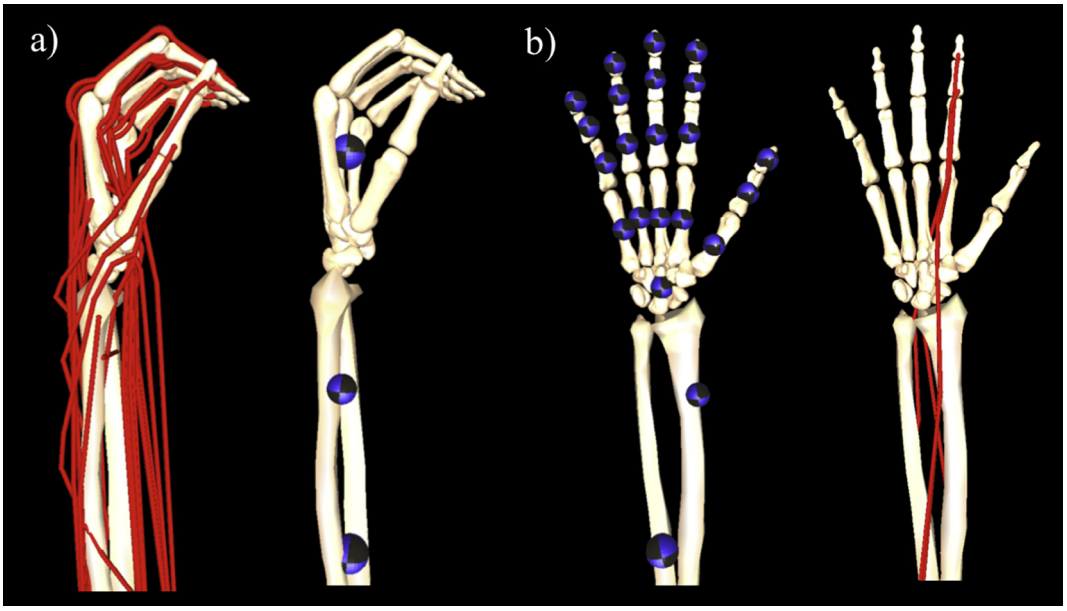

Fig. 1. To enable simulation of combined wrist and finger motions, (a) the kinematic tree of the dynamic model described in Saul et al. (2015) was augmented to (b) include the degrees of freedom and kinematics of the fingers, thumb, and carpal-metacarpal joints. Location of the colored spheres represent the location of center of mass of each individual segment in the distal upper limb within the original model (Saul et al., 2015) and the adapted model; the diameter of each sphere indicates the mass of the modeled segment (see Table 1). Red lines represent simulated muscle-tendon paths within the model; for the purposes of this study, we only included the extrinsic muscles of the index finger. (For interpretation of the references to colour in this figure legend, the reader is referred to the web version of this article.)

et al., 2011; Knutson et al., 2000; O'Driscoll et al., 1992; Richards et al., 1996).

Biomechanical models that are implemented for dynamic simulations of finger movements include passive torques about each finger joint; however, most commonly these models exclude the wrist and distal upper limb (e.g. Babikian et al., 2016; Brook et al., 1995; Esteki and Mansour, 1997; Goislard de Monsabert et al., 2012; Kamper et al., 2002; Li and Zhang, 2009; Sancho-Bru et al., 2003, 2001). While previous simulation work integrating the wrist and hand included active muscle properties that varied with proximal joint posture, the passive viscoelastic torques about each finger joint were defined as a function of a single joint, independent of other joint postures (Adamczyk and Crago, 2000). Here, we incorporate the length-dependent passive forces of the extrinsic index finger muscles into a biomechanical model of the hand and demonstrate their influence on combined passive movements of the wrist and hand.

2. Methods

2.1. Dynamic biomechanical model

A dynamic biomechanical model was developed in OpenSim v3.2 (Delp et al., 2007) by adapting an existing dynamic model of the upper extremity (Saul et al., 2015). The original model included the kinematics of the shoulder, elbow, and wrist, without additional degrees of freedom distal to the wrist. As described previously (Blana et al., 2016), the kinematics of the original model were augmented to include degrees of freedom for digits 1 (thumb) through 5 (pinky finger) (Fig. 1). Mass and inertia properties of the individual hand bone segments were distributed (Le Minor and Rapp, 2001; McFadden and Bracht, 2003) such that the sum of the individual bones are equal to the total mass of the hand segment from Saul et al., 2015 (Table 1). Because critical data needed for the hand model (e.g., passive joint torques) currently only exist for the index finger (digit 2), the simulations of wrist and hand movement described here only involve the index finger. Muscle-tendon paths of the four extrinsic index finger muscles, flexor digitorum superficialis indices (FDSI), flexor digitorum profundus indices (FDPI), extensor digitorum communis indices (EDCI), and extensor indicis proprius (EIP), defined by Saul et al. (2015) were edited so that the moment arms replicated experimental data about the metacarpophalangeal (MCP), proximal-interphalangeal (PIP), and distal-interphalangeal (DIP) joints of the index finger (Fig. 2) (Buford et al., 2005; Fowler et al., 2001).

Passive force-generating properties of the extrinsic muscles were simulated by scaling a generic, Hill-type muscle-tendon model (Millard et al., 2013). Force-generating parameters were taken from Saul et al. with the exception of tendon slack lengths (L_{ts}). L_{ts} was optimized (Table 2) to replicate length-dependent, passive force-generating properties of the extrinsic finger muscles determined experimentally (see Section 2.2). L_{ts} was chosen as the optimization parameter because when all other parameters are held constant for a given muscle-tendon actuator, L_{ts} alters the relationship between joint position and fiber length, influencing the passive muscle forces produced over a given range of joint motion (Arnold et al., 2010; Holzbaur et al., 2005).

Of note, to improve both computational efficiency and numerical stability, the default, normalized, active force-generating curve ($\tilde{f}_a(\tilde{l}_m)$) in the "Millard2012EquilibriumMuscle" model, recommended for general use in OpenSim, yields small active forces at fiber lengths where no active force can be generated (e.g., normalized force = 0.1, 10% of maximum isometric force, at normalized fiber lengths of less than 0.5) (Millard et al., 2013). For similar computational reasons, the default minimum muscle activation is defined as 0.01 (1% of full activation). We altered these default settings, sacrificing computational robustness to enable simulations of purely passive muscle forces (please refer to Appendix A for details). Specifically, the default $\tilde{f}_a(\tilde{l}_m)$ curve in the "Millard2012EquilibriumMuscle" tool in OpenSim 3.2 was modified to replicate the $\tilde{f}_a(\tilde{l}_m)$ curve we have implemented previously (Holzbaur et al., 2005; Saul et al., 2015). Additionally, minimum muscle activation level was defined to be zero. To prevent numerical singularities under these conditions the fiber damping coefficient was defined to be 0.1 (Millard et al., 2013). For consistency, we also modified the default, normalized passive force-length ($\tilde{f}_p(\tilde{l}_m)$) and tendon force-strain ($\tilde{f}_t(\varepsilon_t)$) curves to replicate our previous work.

2.2. Incorporation of the extrinsic finger muscles' length-dependent passive properties

Parameter values for L_{ts} for the four extrinsic finger muscles were defined by solving an optimization problem that matched simulated passive torques about the MCP joint of the index finger to experimental data (Knutson et al., 2000). An optimization algorithm was coded within MATLAB (Natick, MA) to minimize the difference between experimental torques ($T_E(\theta,\omega)$) and the net simulated passive torque ($T_M(\theta,\omega)$) produced by the extrinsic finger muscles, defined as:

$$T_M(\theta,\omega) = \sum_{i=1}^{4} \tilde{f}_{t,i}(\varepsilon_{t,i}(\theta,\omega,L_{ts,i})) \cdot ma_i(\theta) \cdot F_{o,i} \quad (1)$$

where, for the ith actuator: $\tilde{f}_{t,i}(\varepsilon_{t,i}(\theta,\omega,L_{ts,i}))$ is the normalized tendon force at tendon strain ($\varepsilon_{t,i}$), which is a function of MCP angle (θ), wrist angle (ω), and $L_{ts,i}$; ma_i is the moment arm; $F_{o,i}$ is the maximum isometric force.

Table 1
Mass and interial parameters for bone segments.

Segment	Mass (kg)	Center of mass in segment reference frame (m)			Inertia about center of mass (kg m)					
		Rx	Ry	Rz	Ixx	Ixy	Ixz	Iyy	Iyz	Izz
Carpal Bones*	0.3274	−0.0003	0.0033	−0.0045	1.51E−05	0.00E+00	0.00E+00	3.37E−05	0.00E+00	3.96E−05
First metacarpal	0.0160	0.0078	−0.0147	−0.0060	2.38E−06	9.44E−07	5.02E−07	1.42E−06	−8.17E−07	2.52E−06
Second metacarpal	0.0364	0.0000	0.0000	0.0000	9.78E−06	1.45E−06	−2.40E−07	5.29E−07	1.56E−06	9.74E−06
Third metacarpal	0.0381	0.0000	0.0000	0.0000	8.89E−06	1.28E−07	−1.68E−08	2.95E−07	1.12E−06	8.74E−06
Fourth metacarpal	0.0333	−0.0020	−0.0214	0.0034	6.85E−06	−7.04E−07	1.00E−07	3.49E−07	9.37E−07	6.79E−06
Fifth metacarpal	0.0296	−0.0061	−0.0177	0.0054	4.77E−06	−1.06E−06	2.23E−07	5.73E−07	9.36E−07	4.82E−06
Thumb proximal phalanx	0.0079	0.0096	−0.0163	−0.0063	5.21E−07	1.89E−07	7.52E−08	3.19E−07	−1.25E−07	5.85E−07
Thumb distal phalanx	0.0031	0.0056	−0.0104	−0.0044	9.21E−08	2.84E−08	1.31E−08	6.45E−08	−2.09E−08	1.00E−07
Second proximal phalanx	0.0158	0.0044	−0.0253	0.0040	2.41E−06	3.31E−07	−6.25E−08	5.63E−07	3.59E−07	2.40E−06
Second middle phalanx	0.0049	0.0022	−0.0154	0.0002	2.83E−07	2.39E−08	−1.13E−09	7.30E−08	1.01E−08	2.85E−07
Second distal phalanx	0.0018	0.0013	−0.0100	0.0000	4.55E−08	5.53E−09	−5.75E−10	1.58E−08	3.20E−09	4.62E−08
Third proximal phalanx	0.0193	0.0010	−0.0262	0.0037	3.52E−06	8.59E−08	−6.42E−09	6.16E−07	2.17E−07	3.51E−06
Third middle phalanx	0.0064	0.0007	−0.0168	0.0013	5.25E−07	1.99E−08	−8.17E−10	1.01E−07	1.74E−08	5.25E−07
Third distal phalanx	0.0025	0.0005	−0.0102	−0.0003	8.08E−08	4.06E−09	−3.80E−10	2.65E−08	5.10E−09	8.06E−08
Fourth proximal phalanx	0.0137	−0.0022	−0.0238	0.0035	1.95E−06	−2.02E−07	2.31E−08	3.91E−07	1.81E−07	1.96E−06
Fourth middle phalanx	0.0057	−0.0020	−0.0147	0.0012	3.60E−07	−2.37E−08	2.13E−09	9.43E−08	2.41E−08	3.60E−07
Fourth distal phalanx	0.0029	−0.0004	−0.0102	0.0020	9.91E−08	−5.72E−09	1.26E−09	3.64E−08	1.39E−08	9.65E−08
Fifth proximal phalanx	0.0111	−0.0081	−0.0211	0.0021	1.18E−06	−3.28E−07	2.81E−08	3.72E−07	7.93E−08	1.29E−06
Fifth middle phalanx	0.0037	−0.0049	−0.0121	−0.0002	1.57E−07	−4.00E−08	3.69E−09	6.14E−08	1.01E−08	1.70E−07
Fifth distal phalanx	0.0022	−0.0036	−0.0089	0.0003	5.06E−08	−1.24E−08	1.15E−09	2.89E−08	2.53E−09	5.59E−08

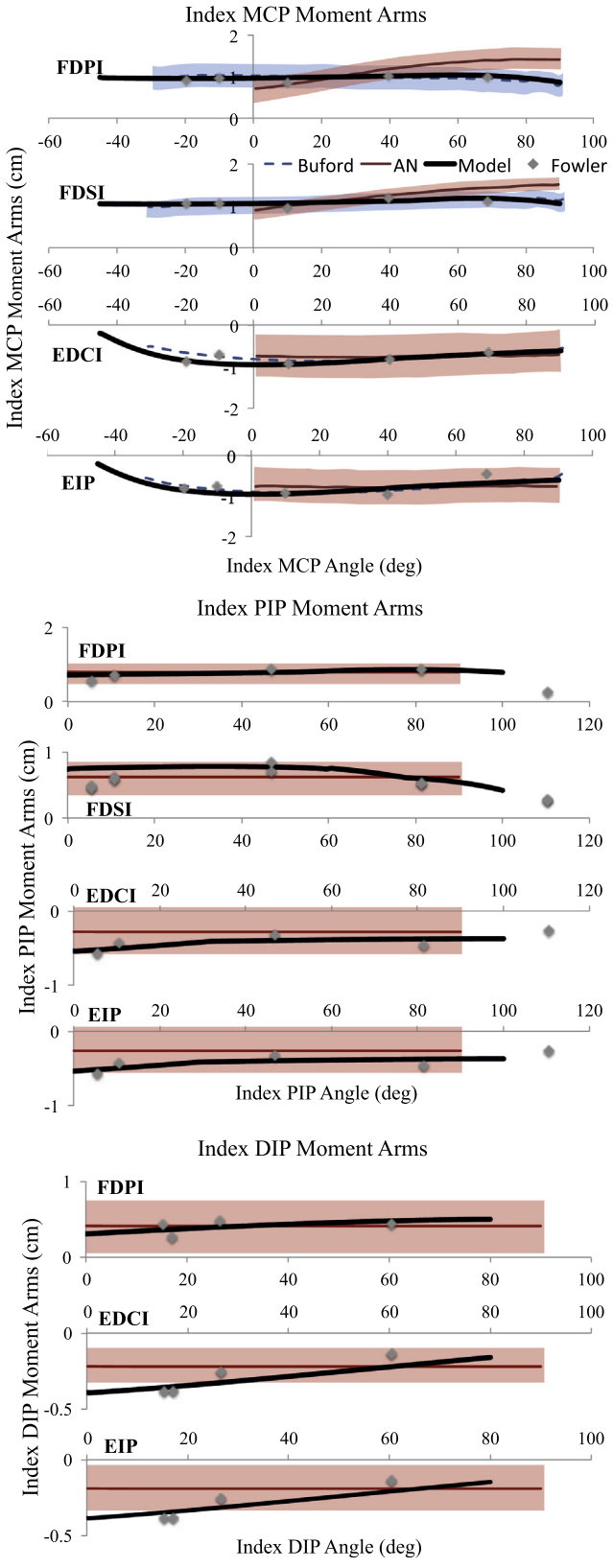

Fig. 2. Moment arm data about the metacarpophalangeal (MCP), proximal interphalangeal (PIP), and distal interphalangeal (DIP) joints of the current model (thick solid black line), Buford et al. (dashed blue line), An et al. (solid red line), and Fowler (grey diamonds) of the flexor digitorum superficialis indices (FDSI), flexor digitorum profundus indices (FDPI), extensor digitorum communis indices (EDCI), and extensor digitorum proprius (EIP) muscles. Shaded area indicates two standard deviations when data was available. (For interpretation of the references to colour in this figure legend, the reader is referred to the web version of this article.)

Table 2
Optimized tendon slack lengths and percent changes.

	FDPI	FDSI	EIP	EDC
Initial tendon slack length	0.3015	0.275	0.21	0.365
New optimized tendon slack length	0.3044	0.2772	0.1911	0.3486
Percent change	0.95%	0.79%	−9.89%	−4.70%

The difference between $T_M(\theta,\omega)$ and $T_E(\theta,\omega)$ was minimized using a 3 degree-of-freedom optimization (Eqs. (2) and (3)), solving for L_{ts} for each of the four extrinsic muscles, subject to a constraint (J), intended to limit changes from initial parameter values.

$$\min[[\sum_{\omega=-60}^{60}\sum_{\theta=-45}^{90}(T_E(\theta,\omega)-T_M(\theta,\omega))^2]+J(L_{ts})] \tag{2}$$

$$J(L_{ts})=\frac{1}{100}\left(\left|\frac{L_{ts,FDSI}-L^I_{ts,FDSI}}{L^I_{ts,FDSI}}-\frac{L_{ts,FDPI}-L^I_{ts,FDPI}}{L^I_{ts,FDPI}}\right|+\left|\frac{L_{ts,EDCI}-L^I_{ts,EDCI}}{L^I_{ts,EDCI}}-\frac{L_{ts,EIP}-L^I_{ts,EIP}}{L^I_{ts,EIP}}\right|\right) \tag{3}$$

L^I_{ts} is the initial tendon slack length from Saul et al. (2015).

For the optimization, passive forces and torques produced by the extrinsic muscles about the MCP joint of the index finger were explicitly calculated in MATLAB (Natick, MA); $\tilde{f}_p(\tilde{l}_m)$ and $\tilde{f}_t(\varepsilon_t)$ curves, all muscle force-generating parameters, muscle-tendon lengths, and moment arms needed for the calculations were exported from the OpenSim v3.2 model.

Normalized passive forces for a given iteration of L_{ts} parameter values were computed by solving a non-linear system of equations (Eqs. (4)–(7)) using the MATLAB *fsolve* function. Each actuator was assumed to be passive and static, simplifying the model to two elastic elements, the tendon and the muscle fibers, arranged in series at a relative orientation specified by the muscle's pennation angle (α). Thus, for all joint postures, muscle fiber length, $L_{m,i}(\theta,\omega)$, and tendon length, $L_{t,i}(\theta,\omega)$, must satisfy:

$$L_{mt,i}(\theta,\omega)=L_{t,i}(\theta,\omega)+\cos(\alpha_i)L_{m,i}(\theta,\omega) \tag{4}$$

where the muscle-tendon length, $L_{mt,i}(\theta,\omega)$, is explicitly defined by the muscle-tendon lengths exported from OpenSim. The force outputs of the muscle and tendon at a given normalized fiber length, $\tilde{l}_{m,i}$, and tendon strain, $\varepsilon_{t,i}$, are specified by the generic $\tilde{f}_p(\tilde{l}_m)$ and $\tilde{f}_t(\varepsilon_t)$ curves exported from OpenSim, and also must satisfy:

$$\tilde{f}_{t,i}(\varepsilon_{t,i}(\theta,\omega,L_{ts,i}))=\cos(\alpha_i)\tilde{f}_{p,i}(\tilde{l}_{m,i}(\theta,\omega)) \tag{5}$$

where $\tilde{l}_{m,i}(\theta,\omega)$ and $\varepsilon_{t,i}(\theta,\omega,L_{ts,i})$ are functions of $L_{m,i}(\theta,\omega)$ and $L_{t,i}(\theta,\omega)$ from Eq. (4), respectively. Specifically,

$$\tilde{l}_{m,i}(\theta,\omega)=\frac{L_{m,i}(\theta,\omega)}{L_{fo,i}} \tag{6}$$

$$\varepsilon_{t,i}(\theta,\omega,L_{ts,i})=\frac{L_{t,i}(\theta,\omega)-L_{ts,i}}{L_{ts,i}} \tag{7}$$

$L_{fo,i}$ is the optimal fiber length.

In passive conditions the muscle-tendon actuator can only generate forces at joint angles where both the tendon is longer than its slack length and the muscle fibers are longer than optimal length. That is:

$$\tilde{f}_{t,i}(\varepsilon_{t,i}(\theta,\omega,L_{ts,i}))=\begin{cases}\tilde{f}_{t,i}(\varepsilon_{t,i}(\theta,\omega,L_{ts,i})) & \text{if } L_{mt,i}(\theta,\omega)\geq L_{ts,i}+\cos(\alpha)L_{fo,i}\\ 0 & \text{otherwise}\end{cases} \tag{8}$$

2.3. Incorporation of passive torques produced by soft tissue structures intrinsic to the hand

The optimization of L_{ts} allows us to simulate passive torques for the extrinsic muscles that replicate the work of Knutson et al. (2000). The net passive torques contributed by the intrinsic soft tissue structures (e.g., ligaments, joint capsules, skin, and intrinsic finger muscles) that cross the MCP, PIP, and DIP joints of the index finger are implemented into the model as three, torsional, spring-dampers, each acting independently about a single joint. In each case, the relationship between passive joint torque and joint angle was specified via the "FunctionBase dBushing" tool (DeMers, 2015) in OpenSim. A cubic spline curve parameterized additional data reported in Knutson et al. (2000) to define the constitutive relationship between the net, passive, elastic torques produced by intrinsic hand structures and MCP joint angle. Similarly, the constitutive torque-angle relationship for the PIP and DIP joints, and the viscous property of each spring-damper acting about the three joints were defined from the literature (Kamper et al., 2002).

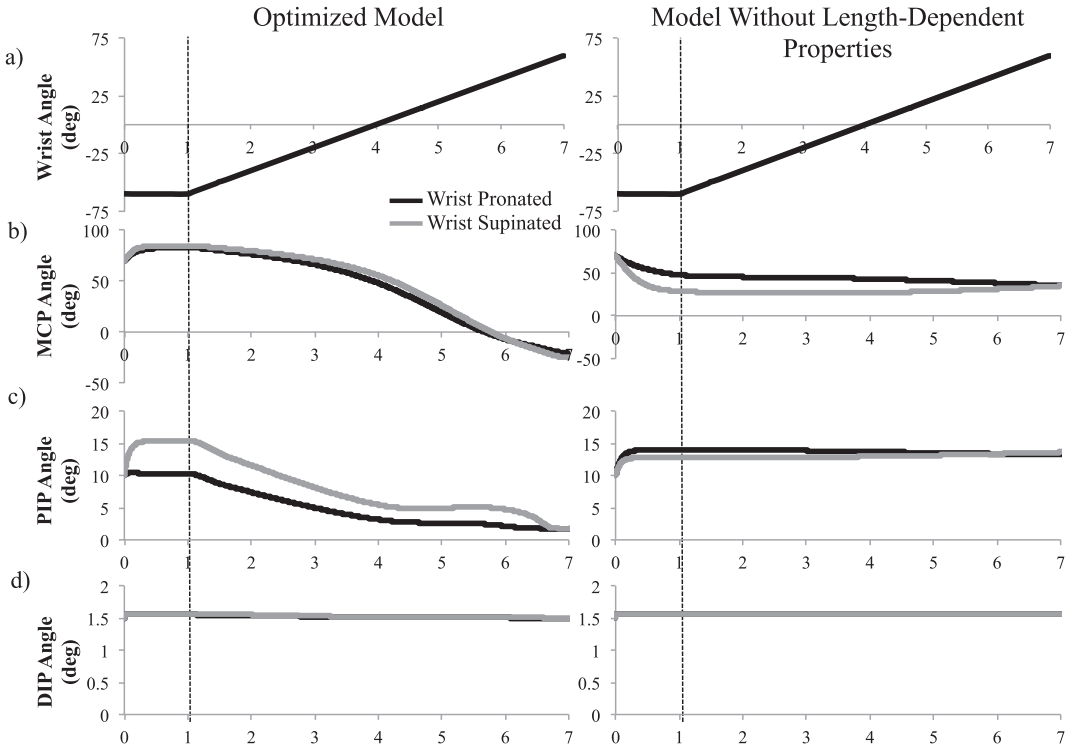

Fig. 3. Wrist and index finger joint postures as a function of time in a pronated (black lines) and supinated (grey lines) forearm position; optimized model results on the left, model without the length-dependent passive properties on the right. (a) Wrist posture was prescribed identically in both sets of simulations, (b) metacarpophalangeal (MCP), (c) proximal interphalangeal (PIP), and (d) distal interphalangeal (DIP) joints postures were simulated. The dotted line indicates start of wrist motion.

2.4. Forward dynamic simulation of wrist and finger motion

Forward dynamic simulations of combined wrist and finger motion were performed in two forearm postures. The hand was oriented horizontally; gravity either opposed (pronated forearm) or assisted (supinated forearm) wrist extension. Wrist motion was prescribed (Fig. 3a). First, 60° extension, maintained for one second, yielded the initial equilibrium position of the index finger. Second, wrist flexion was prescribed at 20°/s, until achieving 60° flexion. The remaining unconstrained degrees of freedom in the model (MCP, PIP, and DIP joint angles) were simulated with time.

Simulations were repeated with all length-dependent passive properties removed from the hand model. In these simulations, passive torques about each finger joint were implemented only by the torsional spring-dampers. Torque magnitudes were re-defined using the sum of the passive torques produced by the intrinsic structures and those produced by the extrinsic finger muscles at a single wrist posture (0° wrist extension).

3. Results and discussion

Simulation of length-dependent passive force-generating properties of extrinsic finger muscles yielded coupled movements between the wrist and index finger during dynamic forward simulations (Fig. 3). With the forearm pronated, prescribed wrist flexion produced coordinated MCP extension (initial position: 83° flexion, final position: 21.8° extension) and PIP extension (11.1–1.7° flexion; Fig. 3b–d), mimicking tenodesis (Johanson and Murray, 2002; Su et al., 2005). With the forearm supinated, the finger joints followed similar trajectories but were more flexed (Fig. 3b–d). Muscle-tendon lengths of the extrinsic finger flexors increase by 1–2% with supination, increasing the passive flexion torques generated. Without length-dependent passive properties, the posture of the index finger was determined by gravity; coupled motion was absent and the finger joints were more extended with the forearm supinated (Fig. 3).

4. Conclusion

Passive torques are critical to achieve controlled and stabilized dynamic free movements of the wrist and fingers (Babikian et al., 2016; Blana et al., 2016; Charles and Hogan, 2012; Kamper et al., 2002). Additionally, passive coupling of the fingers and wrist is a fundamental component of hand function in the severely disabled hand, such as following tetraplegia (Johanson and Murray, 2002; Su et al., 2005). The methods implemented in this study are novel in that they enable incorporation of experimentally measured, length-dependent passive torques produced by the extrinsic muscles in biomechanical models of the hand. Given experimental data for both healthy and impaired hands, the methods described here will enable simulation-based analysis of healthy hand function and evaluation of how musculoskeletal alterations after an injury, that are often associated with increases in passive joint stiffness, affect impaired populations. The extent to which the passive coupling between the hand and distal upper limb joints affects both endpoint force production with the fingers and high-speed movements is unknown; the tools described here facilitate future work in this direction.

Conflict of interest

None.

Acknowledgements

This work was funded by the National Institutes of Health under the Award Numbers R01EB011615, R01HD084009, and T32EB009406. We acknowledge the contributions of Christa Nelson in completing an initial set of simulations that we then expanded to complete the analysis included in the Appendix.

Appendix A. Muscle Model Benchmarking

The current muscle model recommended for general use within the OpenSim v3.0+ software system is the "Millard2012EquilibriumMuscle" tool (Millard et al., 2013). However to improve numerical stability and computational efficiency the default settings of the "Millard2012EquilibriumMuscle" tool in OpenSim yield small active forces at fiber lengths where no active force can be generated. Specifically, normalized fiber lengths of less than 0.5 or greater than 1.5 on the normalized force-length curve produce forces of 10% of maximum isometric force. Physiologically, those normalized lengths should not produce any active force. In addition, the default minimum muscle activation is defined as 0.01 (1% of full activation). Therefore, with the default parameters specified in the "Millard2012EquilibriumMuscle" tool, the model does not simulate 0% muscle activation and the resulting force output includes a force that does not arise from the passive muscle force-length curve.

The purpose of the short communication, that this appendix complements, is to both incorporate the length-dependent passive forces of the extrinsic index finger muscles into a biomechanical model of the upper limb and to demonstrate their influence on combined passive movements of the wrist and hand. In order to generate simulations involving 0% muscle activation and muscle force outputs that only arise from the passive muscle force-length curve we edited the default parameters set in the "Millard2012EquilibriumMuscle" tool in OpenSim v3.2. The parameters were edited to replicate the force generating curves that have been implemented in previous kinematic and dynamic models (Holzbaur et al., 2005; Saul et al., 2015). The previously developed Holzbaur 2005 and Saul 2015 dynamic upper extremity models have been used extensively within and outside of our lab with at least 320 citations between the two models (Web of Science, 2017).

Our edited version of the "Millard2012Equilibrium" muscle model was benchmarked relative to "Muscle Model 4", implemented in the SIMM and Dynamics Pipeline frameworks. Within the Dynamics Pipeline platform, "Muscle Model 4" is an algorithm based on the well-known muscle modeling work described in Lisa Schutte's PhD dissertation (Schutte, 1992).

In order to avoid complications associated with computational challenges that arise when simulating the dynamics of the small masses and inertias of the hand, we evaluated the performance of our edited version of the "Millard2012EquilibriumMuscle" tool in OpenSim by performing the simulations with a musculoskeletal model of the upper extremity isolated to the elbow joint. Identical, simplified musculoskeletal elbow models were implemented within both the SIMM and OpenSim platforms. The models included only 4 muscles; the Triceps Long head, Triceps Lateral head, Biceps Long head, and Biceps Short head. The muscle paths, muscle-tendon geometry, and force generating properties were replicated in both models as described previously (Saul et al., 2015).

A gravity-driven, forward dynamic simulation was performed in each platform to compare the passive behavior of each muscle tool during the simulations. The elbow was initially set to 40 degrees of flexion and then allowed to fall with gravity towards an equilibrium posture. The simulation was run for five seconds. The passive muscle dynamics of the modified "Millard2012EquilibriumMuscle" tool within the OpenSim v3.2 platform were then compared to the passive muscle dynamics of the "Muscle Model 4" tool within the Dynamics Pipeline platform during the gravity driven simulations.

Within both models the long head of the bicep brachii's muscle-tendon unit remains lengthened beyond its slack length throughout the simulation. The muscle-tendon slack length is the length

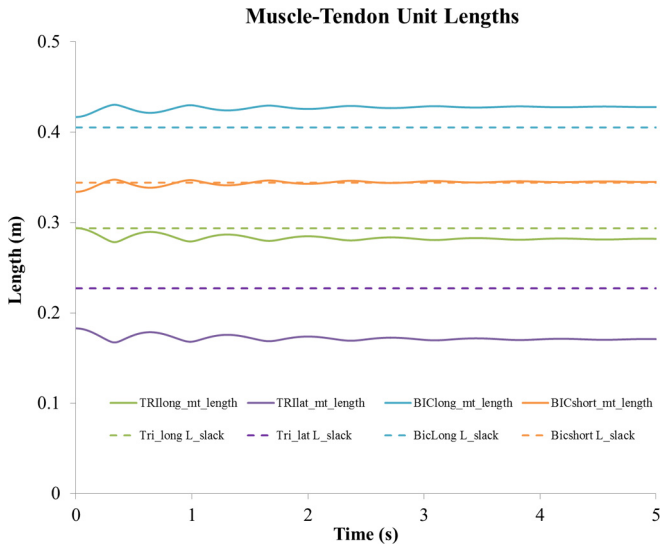

Fig. A.1. Muscle-tendon unit lengths (solid) over time of the triceps long head (green), triceps lateral head (purple), biceps long head (blue), and biceps short head (orange) during the passive forward simulation using the modified "Millard2012EquilbiumMuscle" tool in OpenSim v3.2. The slack length, the length at which passive forces begin, of each muscle is plotted in the dashed lines. (For interpretation of the references to colour in this figure legend, the reader is referred to the web version of this article.)

at which the muscle-tendon unit begins to produce passive forces (Fig. A.1, see also Eq. (8)). The short head of the biceps brachii oscillates about its muscle-tendon slack length. The muscle-tendon lengths of both heads of the triceps remain below the muscle-tendon slack length (Fig. A.1). When the muscle-tendon unit is shorter than the slack length the muscle does not produce passive muscle forces (Eq. (8)). Therefore only the heads of the biceps produce passive forces during this simulation.

The passive dynamic performance of our edited version of the "Millard2012EquilbriumMuscle" tool implemented in OpenSim v3.2 behaves in the same manner as the "Muscle Model 4" implemented in the Dynamics Pipeline. Of interest is the dynamic performance of the muscles producing force, therefore we are only presenting the performance of the biceps and are not presenting the performance of the triceps. In particular, after a brief initialization, the distribution of muscle-tendon length changes between the muscle fiber and the tendon for the biceps is replicated in both tools (Fig. A.2). The length changes of the biceps long head occur primarily in the muscle fiber (Fig. A.2). The length changes of the biceps short muscle depends on whether the muscle-tendon length is longer or shorter than the slack length (Fig. A.2). When the muscle-tendon unit is longer than the slack length the change occurs in muscle fiber. When the unit is shorter than the slack length the change occurs in the tendon and the fiber length remains at the length in which passive forces begin (Fig. A.2).

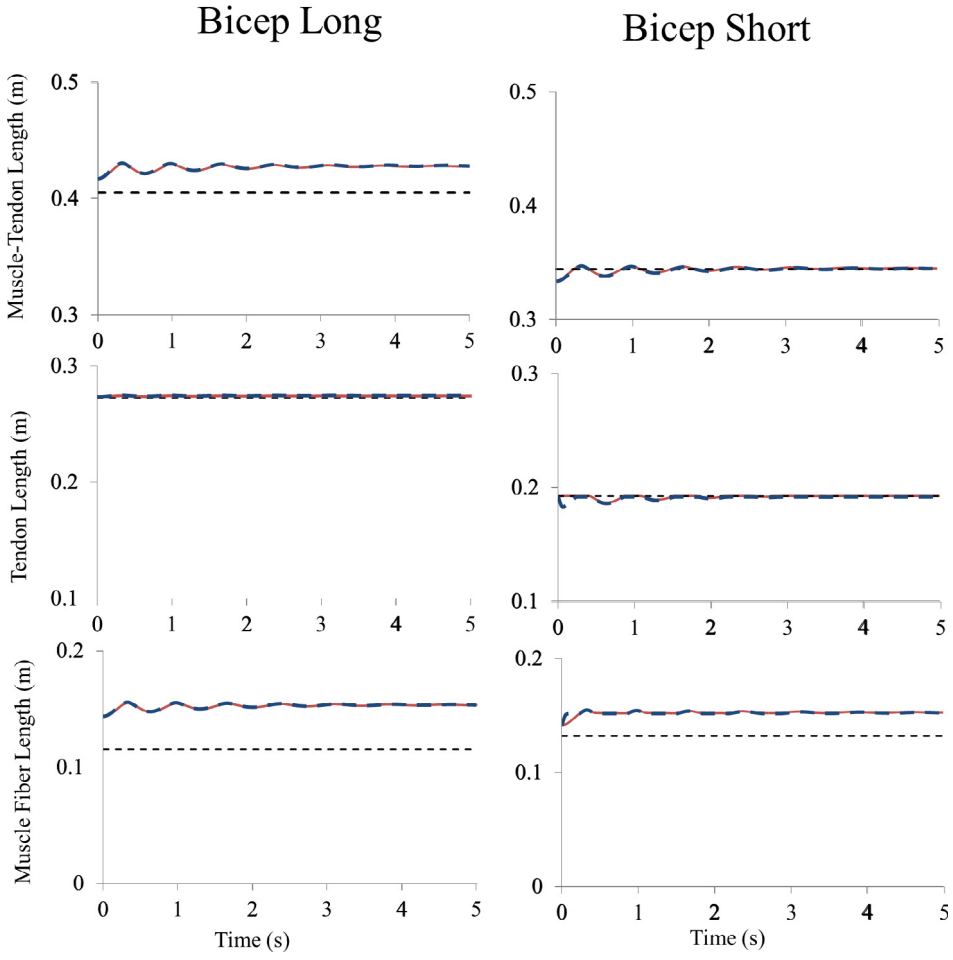

Fig. A.2. The muscle-tendon unit (top), tendon (middle) and muscle fiber (bottom) lengths of the biceps long head (left column) and short head (right column) of the Millard2012Equilibrium tool (red solid) and Muscle Model 4 tool (blue dashed). The slack lengths of the muscle-tendon units, tendons, and muscle fibers (black dashed) are displayed in each graph. (For interpretation of the references to colour in this figure legend, the reader is referred to the web version of this article.)

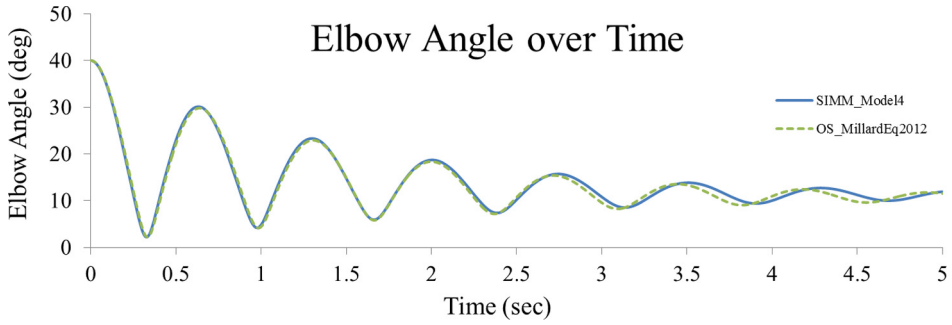

Fig. A.3. Plot of elbow angle over time for a gravity driven simulation within the SIMM and Dynamics Pipline platform using Muscle Model 4 (blue) and the OpenSim platform Millard2012Equilbirum tool (green). (For interpretation of the references to colour in this figure legend, the reader is referred to the web version of this article.)

Given the assumption of no muscle activation or muscle active force for this analysis, the distinct muscle models in the two different software environments default to models of two passive elastic elements, connected in series, in which the tendon is at approximately 20 times stiffer than the muscle fibers. By definition, when the muscle-tendon unit is longer than its slack length the fiber and tendon are also lengthened beyond their slack lengths. Due to the relatively high tendon stiffness, passive length changes occur in the muscle fibers with relatively little concomitant change in tendon length. This expected behavior is observed in both biceps muscles during the simulations, in both platforms (Fig. A.2).

The resultant system dynamics of the musculoskeletal model show that the elbow angle over time using each muscle tool match well (R^2=0.989, RMSE=0.711 over the whole time period) (Fig. A.3). The simulations are nearly identical for the first 2.5 seconds (R^2=0.997, RMSE=0.506 for seconds 0 to 2.5). After 2.5 seconds the joint posture between the models deviate (R^2=0.794, RMSE=0.870 for seconds 2.5 to 5). These differences likely occur due to numerical differences during the calculation of muscle force between the two tools and platforms. As the simulations continue these differences propagate and lead to the increasingly different joint angles.

We conclude that the parameter changes we implemented to enable simulations of purely passive muscle forces produce acceptable results, consistent with two elastic elements of varied stiffness connected in series, and replicated when the same parameters are implemented in a different muscle model in a different software platform. Minimal differences in the outputs of the muscle model are observed over a 5 second simulation, as evidenced in Figs. A.2 and A.3. The main caveats to our implementation are associated with computational robustness: using the default parameters of the "Millard2012EquilbirumMuscle" tool yields faster computation times, and increases computational stability. Our modifications increase the computation time of the simulations and introduce the potential that the muscle tool may become unstable and crash during dynamic simulations; however we did not experience any crashes during the dynamic simulations at the hand or elbow. These trade-offs were necessary for the purposes of this paper.

References

Adamczyk, M.M., Crago, P.E., 2000. Simulated feedforward neural network coordination of hand grasp and wrist angle in a neuroprosthesis. IEEE Trans. Rehabil. Eng. 8, 297–304.

Arnold, E.M., Ward, S.R., Lieber, R.L., Delp, S.L., 2010. A model of the lower limb for analysis of human movement. Ann. Biomed. Eng. 38, 269–279.

Babikian, S., Valero-Cuevas, F.J., Kanso, E., 2016. Slow movements of bio-inspired limbs. J. Nonlinear Sci. 26, 1293–1309.

Bhardwaj, P., Nayak, S.S., Kiswar, A.M., Sabapathy, S.R., 2011. Effect of static wrist position on grip strength. Indian J. Plast. Surg. 44, 55–58.

Blana, D., Chadwick, E., van den Bogert, A.J., Murray, W.M., 2016. Real-time simulation of hand motion for prosthesis control. Comput. Method Biomech. (in press).

Brook, N., Mizrahi, J., Shoham, M., Dayan, J., 1995. A biomechanical model of index finger dynamics. Med. Eng. Phys. 17, 54–63.

Buford Jr., W.L., Koh, S., Andersen, C.R., Viegas, S.F., 2005. Analysis of intrinsic-extrinsic muscle function through interactive 3-dimensional kinematic simulation and cadaver studies. J. Hand Surg. Am. 30, 1267–1275.

Charles, S.K., Hogan, N., 2012. Stiffness, not inertial coupling, determines path curvature of wrist motions. J. Neurophysiol. 107, 1230–1240.

Delp, S.L., Anderson, F.C., Arnold, A.S., Loan, P., Habib, A., John, C.T., Guendelman, E., Thelen, D.G., 2007. OpenSim: open-source software to create and analyze dynamic simulations of movement. IEEE Trans. Biomed. Eng. 54, 1940–1950.

DeMers, M., 2015. OpenSim::FunctionBasedBushingForce Class Reference.

Esteki, A., Mansour, J.M., 1997. A dynamic model of the hand with application in functional neuromuscular stimulation. Ann. Biomed. Eng. 25, 440–451.

Fowler, N.K., Nicol, A.C., Condon, B., Hadley, D., 2001. Method of determination of three dimensional index finger moment arms and tendon lines of action using high resolution MRI scans. J. Biomech. 34, 791–797.

Goislard de Monsabert, B., Rossi, J., Berton, E., Vigouroux, L., 2012. Quantification of hand and forearm muscle forces during a maximal power grip task. Med. Sci. Sports Exerc. 44, 1906–1916.

Holzbaur, K.R., Murray, W.M., Delp, S.L., 2005. A model of the upper extremity for simulating musculoskeletal surgery and analyzing neuromuscular control. Ann. Biomed. Eng. 33, 829–840.

Hooper, S.L., Guschlbauer, C., Blumel, M., Rosenbaum, P., Gruhn, M., Akay, T., Buschges, A., 2009. Neural control of unloaded leg posture and of leg swing in stick insect, cockroach, and mouse differs from that in larger animals. J. Neurosci.: Off. J. Soc. Neurosci. 29, 4109–4119.

Johanson, M.E., Murray, W.M., 2002. The unoperated hand: the role of passive forces in hand function after tetraplegia. Hand Clin. 18, 391–398.

Kamper, D.G., Hornby, G.T., Rymer, W.Z., 2002. Extrinsic flexor muscles generate concurrent flexion of all three finger joints. J. Biomech. 35, 1581–1589.

Knutson, J.S., Kilgore, K.L., Mansour, J.M., Crago, P.E., 2000. Intrinsic and extrinsic contributions to the passive moment at the metacarpophalangeal joint. J. Biomech. 33, 1675–1681.

Kuo, P.H., Deshpande, A.D., 2012. Muscle-tendon units provide limited contributions to the passive stiffness of the index finger metacarpophalangeal joint. J. Biomech. 45, 2531–2538.

Le Minor, J.M., Rapp, E., 2001. Relative weights of the human carpal bones: biological and functional interests. Ann. Anat. 183, 537–543.

Li, K., Zhang, X., 2009. A novel two-stage framework for musculoskeletal dynamic modeling: an application to multifingered hand movement. IEEE Trans. Biomed. Eng. 56, 1949–1957.

McFadden, D., Bracht, M.S., 2003. The relative lengths and weights of metacarpals and metatarsals in baboons (*Papio hamadryas*). Horm. Behav. 43, 347–355.

Millard, M., Uchida, T., Seth, A., Delp, S.L., 2013. Flexing computational muscle: modeling and simulation of musculotendon dynamics. J. Biomech. Eng. 135, 021005.

Mirakhorlo, M., Visser, J.M.A., Goislard de Monsabert, B.A.A.X., van der Helm, F.C.T., Maas, H., Veeger, H.E.J., 2016. Anatomical parameters for musculoskeletal modeling of the hand and wrist. Int. Biomech. 3, 40–49.

O'Driscoll, S.W., Horii, E., Ness, R., Cahalan, T.D., Richards, R.R., An, K.N., 1992. The relationship between wrist position, grasp size, and grip strength. J. Hand Surg. Am. 17, 169–177.

Richards, L.G., Olson, B., Palmiter-Thomas, P., 1996. How forearm position affects grip strength. Am. J. Occup. Ther. 50, 133–138.

Sancho-Bru, J.L., Perez-Gonzalez, A., Vergara, M., Giurintano, D.J., 2003. A 3D biomechanical model of the hand for power grip. J. Biomech. Eng. 125, 78–83.

Sancho-Bru, J.L., Perez-Gonzalez, A., Vergara-Monedero, M., Giurintano, D., 2001. A 3-D dynamic model of human finger for studying free movements. J. Biomech. 34, 1491–1500.

Saul, K.R., Hu, X., Goehler, C.M., Vidt, M.E., Daly, M., Velisar, A., Murray, W.M., 2015. Benchmarking of dynamic simulation predictions in two software platforms using an upper limb musculoskeletal model. Comput. Methods Biomech. Biomed. Eng. 18, 1445–1458.

Schutte, L.M., 1992. Using Musculoskeletal Models to Explore Strategies for Improving Performance in Electrical Stimulation-Induced Leg Cycle Ergometry. Stanford Univeristy, Palo Alto.

Souza, T.R., Fonseca, S.T., Goncalves, G.G., Ocarino, J.M., Mancini, M.C., 2009. Prestress revealed by passive co-tension at the ankle joint. J. Biomech. 42, 2374–2380.

Su, F.C., Chou, Y.L., Yang, C.S., Lin, G.T., An, K.N., 2005. Movement of finger joints induced by synergistic wrist motion. Clin. Biomech. (Bristol, Avon) 20, 491–497.

Web Of Science, February 10, 2017. Times Cited.

Wu, M.M., Pai, D.K., Tresch, M.C., Sandercock, T.G., 2012. Passive elastic properties of the rat ankle. J. Biomech. 45, 1728–1732.